Eur. Phys. J. E (2024)47:17
https://doi.org/10.1140/epje/s10189-024-00410-1

THE EUROPEAN PHYSICAL JOURNAL E

Regular Article - Flowing Matter

Viscosimetric squeeze flow of suspensions

K. Zidi, B. Darbois Texier, G. Gauthier, and A. Seguin[a]

Université Paris-Saclay, CNRS, Laboratoire FAST, 91405, Orsay, France

Received 26 September 2023 / Accepted 12 February 2024

Abstract The rheology of particle suspensions has been extensively explored in the case of a simple shear flow, but less in other flow configurations which are also important in practice. Here we investigate the behavior of a suspension in a squeeze flow, which we revisit using local pressure measurements to deduce the effective viscosity. The flow is generated by approaching a moving disk to a fixed wall at constant velocity in the low Reynolds number limit. We measure the evolution of the pressure field at the wall and deduce the effective viscosity from the radial pressure drop. After validation of our device using a Newtonian fluid, we measure the effective viscosity of a suspension for different squeezing speeds and volume fractions of particles. We find results in agreement with the Maron–Pierce law, an empirical expression for the viscosity of suspensions that was established for simple shear flows. We prove that this method to determine viscosity remains valid in the limit of large gap width. This makes it possible to study the rheology of suspensions within this limit and therefore suspensions composed of large particles, in contrast to Couette flow cells which require small gaps.

1 Introduction

Many natural events and industrial processes involve the flow of suspensions made of solid particles dispersed in a fluid. This is the case of mudflows [1], handling of fresh concrete [2] or food processing [3]. This context has motivated an intense research activity in the field of dense suspensions rheology, with a particular emphasis on the case of simple shear flows [4]. Most of the rheological studies of suspensions have been realized in the Couette flow cells of rheometers which requires small gaps. This point prevents the study of suspensions composed of large particles, which are often encountered in the applications. It is therefore necessary to develop new rheological configurations that are not limited to small gap widths.

Since Einstein's pioneering work [5], the law of suspension viscosity $\eta(\phi)$, where ϕ is the particle volume fraction, has been extended by Batchelor to take into account the hydrodynamic interactions between two particles [6]. Beyond the dilute regime the expressions of Einstein and Batchelor are valid, several empirical expressions have been proposed to account for the viscosity of suspensions. One of the most used is the Maron–Pierce law which describes the relative viscosity of the suspension $\eta_r(\phi) = \eta(\phi)/\eta_f$ according to the relation:

$$\eta_r(\phi) = \left(1 - \frac{\phi}{\phi_c}\right)^{-2} \tag{1}$$

where η_f is the viscosity of the Newtonian carrier fluid and ϕ_c is a critical volume fraction ranging from 0.58 to 0.66. The large range of ϕ_c for which the viscosity diverges - i.e., the suspension becomes solid - has drawn the attention of several studies [7,8]. The commonly assumed origins of the variations in volume fraction for the transition between fluid and solid are the roughness of the particles [9] or their size dispersion [10–13]. In the flowing regime, the strong increase in the relative viscosity at moderate and large volume fractions has been shown to mainly result from frictional contacts between particles and depends of their spatial arrangement [14,15]. Depending on how the frictional contacts between particles are mobilized when the suspension flows, several phenomena can occur such as shear-thinning [16], shear-thickening [17], shear-induced migration [18] and normal stress differences [19]. The investigation of normal stress differences in various flow configurations revealed disparities in intensity [20–22] and in the sign [21,23]. These observations show the strong influence of the flow configuration on the behavior of the suspension. This can be attributed to the fact that different types of solicitation lead to different micro-structures of the suspension. This context

[a] e-mail: antoine.seguin@universite-paris-saclay.fr (corresponding author)

Published online: 01 March 2024

raises the question of the behavior of a macroscopic suspension in a squeeze flow configuration where the shear rate is non-homogeneous and where the micro-structure may differ from the case of a simple shear flow. This question is essential to determine whether the squeeze flow configuration can be used as a rheological configuration for studying suspensions.

Compared to simple shear flows, suspensions in squeeze flows, have been less studied (see [24] for a review). For this compression-type solicitation, the different studies have mainly considered the global force experienced by the moving disk, and the effective viscosity deduced from this measurement is global because it is integrated over the surface of the disk. In addition, these experiments are often realized with a small volume of suspension between the plates [25], which creates capillary interfaces that prevent drainage but can affect the squeeze flow. For a zeolite suspension of volume fraction between 5 and 20 %, the required squeezing force corresponds to the one expected for a Newtonian fluid of viscosity equivalent to the effective viscosity of the suspension [26]. It is no more the case at large volume fractions ($\phi > 0.40$) and for suspending fluids of low viscosities ($\eta_f < 1$ Pa.s), where a different flow regime has been identified. In this case, the suspending fluid filtered through particles and induced a more concentrated region of particles in the center [27,28]. The consequences of flow filtration have been observed in the measurements of the normal stress distribution made with pressure-sensitive films in a suspension undergoing constant-force squeeze flow [29]. They observed that above 55% in volume fraction, the normal stress profile deviated from the Newtonian prediction and was larger in the central region and lower at the edge. This pressure distribution was interpreted as the result of jamming in the central zone. However, these previous studies do not consider the intermediate case where the suspension is concentrated but where no filtration occurs and the squeeze flow can be used as a rheological configuration to measure the effective viscosity of the suspension.

In this paper, using an experimental setup soliciting a fluid in compression, we revisit the rheology of the suspension in the squeeze flow configuration to investigate the behavior of suspension in a non simple shear flow and in the limit of large gap widths. We measure the effective viscosity of the suspension through local pressure sensors. After developing the theoretical framework of our non-viscosimetric flow, in which we describe the velocity field and the pressure field analogously, we deduce a global relation allowing to measure the effective viscosity of the fluid. Then we validate our experimental protocol on a Newtonian fluid and we apply it to deduce the effective viscosity of a suspension. The dependence with the particle volume fraction of the measured relative viscosity of the suspensions is in agreement with the empirical law of Maron–Pierce established for simple shear flows.

2 Experimental setup

2.1 Suspension

The suspensions were prepared mixing polystyrene particles (Microbeads TS 500) with Poly(ethylene glycol-ran-propylene glycol) monobutyl ether (PEG) from Sigma-Aldrich, of viscosity $\eta_f = 2.9 \pm 0.1$ Pa.s and density $\rho_f = 1050$ kg.m^{-3} that matches the nominal density of the polystyrene particles at 20 °C. The rheology of the suspending fluid was confirmed to be Newtonian over the shear rate range $[0.01 - 100\,\mathrm{s}^{-1}]$ using cylindrical Couette cell of internal radius $R_i = 13.33$ mm and intergap of $0.085\,R_i$ (Anton Paar MCR 501), with a dynamic viscosity of $\eta_f = 2.90 \pm 0.02$ Pa.s at 20 °C. The polystyrene particles are smooth, rather monodispersed, spherical with a diameter of $a = 500 \pm 40\,\mu$m. The suspensions were prepared by agitating the particles in a planetary mixer (Kenwood KCL95), gradually adding the suspending fluid, and mixing for 10 to 15 min. The suspension was then passed through a vacuum bell jar to remove air bubbles. This protocol allows to prepare homogeneous suspensions with volume fractions $\phi = [0.3 - 0.5]$. The rheology of these suspensions was characterized in the same cylindrical Couette cell (Anton Paar MCR 501) used for the carrier fluid. As the intergap of the cylindrical cell is 1.13 mm, we studied the same suspension but made with particles of 80 μm in size in order to avoid particle size effects in the gap. We observe that the viscosity of suspensions increases with the volume fraction in agreement with the prediction given by Eq. (1) leading to $\phi_c = 0.62 \pm 0.01$. This value of ϕ_c is in the range of usual values ($0.58 < \phi_c < 0.66$) reported in a review [4]. This review also reports there is no systematic effect of the grain size on ϕ_c (from 40 μm up to 1100 μm).

2.2 Squeeze flow

The squeeze flow is generated into a rectangular reservoir filled with the fluid (total volume is 5 L) where an immersed disk of 150 mm in diameter approaches a vertical wall of the reservoir (see Fig. 1a). The horizontal motion of the disk is imposed by a linear stage (Physik Instrumente M-414) that permits to control the moving velocity V_0 and the separating distance H between the disk with the vertical wall. The parallelism between the disk and the wall is ensured with an angle lower than 1.2 °. In order to measure the fluid pressure P during the squeeze flow, the wall was instrumented with two pressure sensors (Keller PR-25) that have a resolution of ±2 Pa. The first sensor was installed along the central axis of the moving disk and measure the pressure P_1 at this location. The second sensor is placed at a distance $R = 60$ mm from the central axis and measure the pressure P_2. The signals P_1 and P_2 were registered as

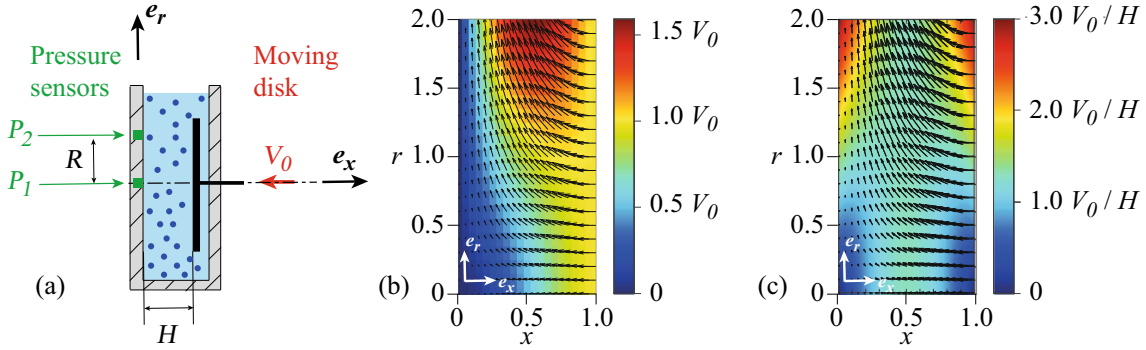

Fig. 1 **a** Sketch of the experimental setup: a moving disk is squeezing the suspension at a constant velocity V_0 along $\mathbf{e}_x$. Pressure sensors are located on the opposite wall in order to measure the pressure difference $P_1 - P_2$. **b** Velocity field associated to the squeeze flow deduced from Eqs. (7) and (8). The color map represents the norm of the velocity. **c** Shear rate field associated to the squeeze flow according to Eqs. (7) and (8). The color map represents the shear rate calculated from Eq. (13). The black arrows represent the velocity field as in figure b

a function of time with a sampling frequency of 100 Hz and synchronized with the displacement of the disk as it approaches the instrumented wall. In all experiments, the initial and final separating distances were $H = 47.6$ mm and $H = 10.0$ mm, respectively. The velocity range explored was $V_0 = [0.5 - 10]\,\mathrm{mm \cdot s^{-1}}$ and ensured that the Reynolds number based on the separating distance H, $\mathrm{Re} = \rho_f V_0 H/\eta_s$, was smaller than 10^{-1} even for experiments at $\phi = 0$ (pure suspending fluid).

3 Viscosimetry

3.1 Effective viscosity model

In this section, we describe the ideal case of a Newtonian liquid, of constant viscosity η and density ρ, squeezed between two disks of diameter D which are approaching each other at the relative velocity V_0. Numerous studies have addressed this problem theoretically [30–33] and here we only recall the main calculation steps that allow us to derive a measure of the effective viscosity in this configuration in the limit of low Reynolds numbers.

The problem is parametrized in a cylindrical frame of reference $(0, \mathbf{e}_x, \mathbf{e}_r, \mathbf{e}_\theta)$ where $(\mathbf{e}_r, \mathbf{e}_\theta)$ is the vertical plane (Fig. 1a). At the edge of the disks, the pressure applied by the rest of the fluid in the tank is considered to be constant. The flow is assumed to be stationary and in the limit of low Reynolds number, $Re = \rho V_0 H/\eta < 0.1$, so that the advection terms in the equilibrium equation are neglected. Far from the edges of the disk, the quasi-static velocity field $\mathbf{V}$ in this axisymmetric geometry can be written: $\mathbf{v}(x,r) = \mathbf{V}/V_0 = v_x(x,r)\mathbf{e}_x + v_r(x,r)\mathbf{e}_r$ where x and r are the cylindrical coordinates normalized by the distance H. The pressure field $P(x,r)$ is normalized by the stress scale $3\eta V_0/H$ to get the non-dimensional pressure $p(x,r) = P(x,r)H/3\eta V_0$. In this configuration, the conservation of momentum is similar to the Stokes equation (neglecting the volume force terms):

$$0 = -3\frac{\partial p}{\partial x} + \left(\frac{\partial^2 v_x}{\partial r^2} + \frac{1}{r}\frac{\partial v_x}{\partial r} + \frac{\partial^2 v_x}{\partial x^2}\right) \tag{2}$$

$$0 = -3\frac{\partial p}{\partial r} + \left(\frac{\partial^2 v_r}{\partial r^2} + \frac{1}{r}\frac{\partial v_r}{\partial r} - \frac{v_r}{r^2} + \frac{\partial^2 v_r}{\partial x^2}\right) \tag{3}$$

The incompressibility of the flow ($\nabla \cdot \mathbf{v} = 0$) allows to define the existence of a stream function $\psi(x,r)$ such that:

$$v_x(x,r) = -\frac{1}{r}\frac{\partial \psi}{\partial r} \qquad v_r(x,r) = \frac{1}{r}\frac{\partial \psi}{\partial x} \tag{4}$$

Using the stream function $\psi(r,x)$ and cross differentiating Eqs. (2) and (3) in order to eliminate pressure p, it leads to the equation:

$$\begin{aligned} 0 \;=\; & \frac{1}{r}\left(\frac{\partial^4 \psi}{\partial r^4} + \frac{\partial^4 \psi}{\partial x^4} + 2\frac{\partial^4 \psi}{\partial r^2 \partial x^2}\right) \\ & - \frac{2}{r^2}\frac{\partial}{\partial r}\left(\frac{\partial^2 \psi}{\partial x^2} + \frac{\partial^2 \psi}{\partial r^2}\right) + \frac{3}{r^3}\frac{\partial^2 \psi}{\partial r^2} - \frac{3}{r^4}\frac{\partial \psi}{\partial r} \end{aligned} \tag{5}$$

Equation (5) admits a solution of the form $\psi(r,x) = r^2\lambda(x)$ which results in an equation on λ:

$$0 = \frac{d^4\lambda}{dx^4} \tag{6}$$

The velocity boundary conditions on the fixed wall are defined by $v_x(0,r) = 0$ and $v_r(0,r) = 0$. The boundary conditions on the moving wall are $v_x(1,r) = -1$ and $v_r(1,r) = 0$. By combining Eqs. (4) and (6), the velocity field, solution of the problem is:

$$v_x(x) = -x^2(3 - 2x) \tag{7}$$

$$v_r(x,r) = 3rx(1 - x) \tag{8}$$

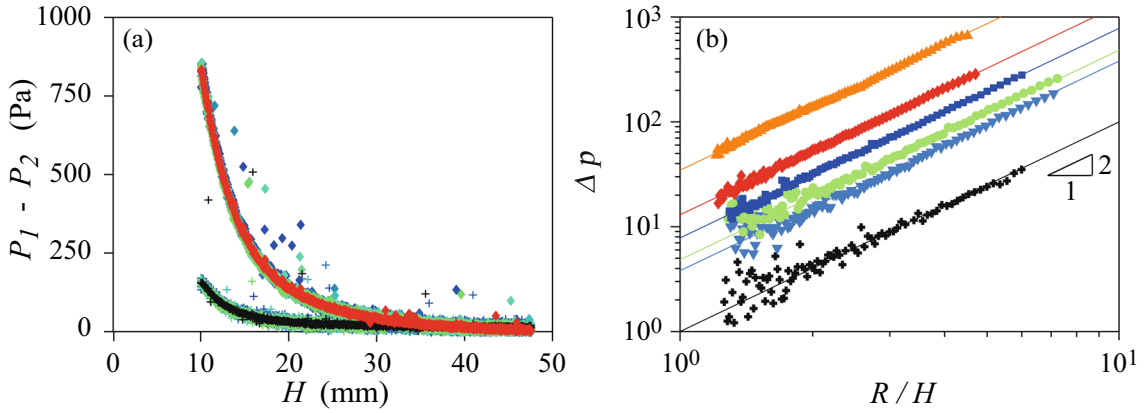

Fig. 2 **a** Pressure difference $\Delta P = P_1 - P_2$ as a function of H for pure fluid (lower curve) and suspension of $\phi = 0.45$ (upper curve). The imposed velocity is: $V_0 = 4$ mm $\cdot$ s^{-1}. The data has been collected on ten successive realizations (data points ranging from turquoise to blue). The mean of these realizations have been plotted with symbol (+) for the pure fluid and with symbol ($\diamond$) for suspension. **b** Normalized pressure difference Δp of the pure fluid and suspension as a function of H/R. For the pure fluid, the symbols (+) are experimental data and the dark solid line corresponds to theoretical prediction given by Eq. (10). For suspension, the symbols are experimental data ($\blacktriangledown$) $\phi = 0.30$, ($\bullet$) $\phi = 0.35$, ($\blacksquare$) $\phi = 0.40$, ($\blacklozenge$) $\phi = 0.45$ and ($\blacktriangle$) $\phi = 0.50$. The colored solid lines correspond to theoretical prediction of Eq. (12) where η_r is fitted by least mean square method

Once the normalized velocity field has been determined, it is possible to determine the pressure field by integration of Eqs. (2) and (3):

$$p(x, r) = \left(-r^2 - 2x\,(1 - x)\right) + p_0 \tag{9}$$

where p_0 is an integration constant. Equation (9) allows to deduce that the normalized pressure difference $\Delta p = p(0, 0) - p(0, R/H)$ between the center of the flow and the periphery expresses:

$$\Delta p = \left(\frac{R}{H}\right)^2. \tag{10}$$

In a dimensional form, Eq. (10) writes:

$$\Delta P = \frac{3\eta V_0 R^2}{H^3}. \tag{11}$$

This relation means that from the measurement of the pressure difference $\Delta P = P_1 - P_2$ made with the two pressure sensors located at a distance R on the fixed wall of the experimental setup and knowing the velocity V_0 of the moving disk and the separating distance H, one can deduce the viscosity η of the fluid. Note that Eq. (11) has been established without considering lubrication approximation implying $H/R \ll 1$, as already mentioned in [24].

3.2 Validation with a Newtonian fluid

In order to validate our experimental setup, we realized a set of measurements with the pure Newtonian suspending fluid ($\eta_f = 2.9 \pm 0.1$ Pa.s) squeezed in our setup at a velocity $V_0 = 4$ mm $\cdot$ s^{-1}. The corresponding pressure difference $P_1 - P_2$ is shown as a function of the separating distance H in Fig. 2a ((+), lower curve). We first observe that the pressure difference is vanishingly small at large separation distances and increases drastically as the disk approaches the wall. We also observe there is no drift of the pressure during ten successive compression cycles. The pressure profiles remain similar and thus can be averaged over 10 cycles in order to obtain a unique pressure profile. Then, we present the normalized value Δp deduced from this signal as a function of R/H, (+) in Fig. 2b. The pressure difference has been normalized using the value of the viscosity measured in the rheometer. The dark solid line in Fig. 2b represents the prediction of Eq. (10) and a good agreement between experiments and theory is observed with no fitting parameters. Note that this agreement is valid for the whole range of aspect ratio H/R as expected and also reported in [24]. Thus, the measurement of the radial pressure drop in a squeeze flow allows to deduce the dynamic viscosity of the fluid that is squeezed.

3.3 Effective viscosity of suspension

We performed similar experiments with suspensions of polystyrene particles squeezed at constant speed. Figure 2b shows the evolution of the normalized pressure difference Δp as a function of R/H for a compression speed $V_0 = 4\,\text{mm} \cdot \text{s}^{-1}$ and different volume fractions ϕ. We observed that the normalized pressure difference scales as $\Delta p \sim (R/H)^2$ as for a Newtonian fluid but with a prefactor that increases with ϕ. For a suspension of relative viscosity η_r, the normalized pressure difference, Eq. (10), reads:

$$\Delta p = \eta_r(\phi) \left(\frac{R}{H}\right)^2. \quad (12)$$

According to this expression, the prefactor that can be extracted from the logarithmic plot in Fig. 2b corresponds directly to the relative viscosity of the suspension η_r. Experiments have been conducted with suspensions of various particle volume fraction $0.3 \leq \phi \leq 0.5$ and for different compression velocities V_0 ranging from 0.5 to 10 mm $\cdot$ s^{-1}. The relative viscosity $\eta_r(\phi)$ deduced from these experiments are displayed in Fig. 3, as a function of ϕ (the different colors correspond to different velocities V_0). We observe that the relative viscosity of the suspension has no clear dependence on the squeezing speed for each particle volume fraction ϕ. In this configuration, we do not observe a significant shear thinning effect [21]. Thus, for each ϕ we average the relative viscosity over different compression velocities. The inset of Fig. 3 shows the increase of the relative viscosity with the particle volume fraction. The best fit of the evolution $\eta_r(\phi)$ with the Maron–Pierce law given by Eq. (1) is found for $\phi_c = 0.61 \pm 0.02$. This value is equal to the value estimated from rheological measurements detailed in Sect. 2.1. Moreover it is in agreement with the set of values found in previous studies [4].

3.4 Discussion

Measurements of suspension viscosity in rheometer faces different issues such as particle size effects, shear-induced migration and particle wall slip that are not predominant in squeeze flow configuration. Conversely, the drawback of squeeze flow is the liquid/solid separation that gives rise to shear jamming, but which is not observed here. We discuss in the following these different issues in cylindrical Couette rheometers and homemade squeeze flows.

Most Couette rheometers use gaps of the order of 1 mm. Thus, in order to have enough particles in the gap ($>$ 10), it is difficult to characterize suspensions whose particles have a diameter > 100 µm. One advantage of the present setup is that it can be used to characterize suspensions of particles up to 1 mm in diameter, although this requires a larger volume of suspension than Couette rheometers.

Moreover, the squeeze flow presents by nature large shear gradients that might lead to particles migration. The intensity of this phenomenon must be estimated because it can affect the hypothesis of homogeneous suspension considered in the theoretical analysis. The shear rate inhomogenity can be estimated by defining the shear rate $\dot{\gamma}$ as the second invariant of the strain rate tensor [34]. From Eqs. (7) and (8) for the velocity field, the normalized shear rate writes:

$$\dot{\gamma}(x,r) = \frac{3}{2}\left(12x^2(x-1)^2 + r^2(2x-1)^2\right)^{1/2} \quad (13)$$

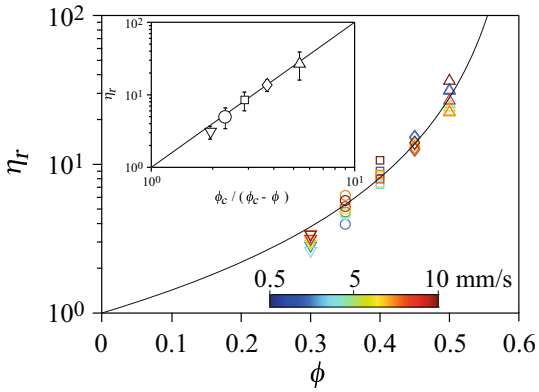

Fig. 3 Relative viscosity of the suspension versus the particle volume fraction ϕ in semi-log scale. The imposed velocity V_0 ranges from 0.5 up to 10 mm$\cdot$ s^{-1} and the magnitude of the velocity is in agreement with the colorbar. The solid line corresponds $\eta_r = (\phi_c/(\phi_c - \phi))^2$ with $\phi_c = 0.61$. Inset: Relative viscosity of the suspension versus reduced volume fraction $(\phi_c/(\phi_c - \phi))$. Each symbol is the average of the relative viscosity for the different velocities

The predictions of Eq. (13) for the normalized shear rate are plotted with a color map in Fig. 1c. We observe that the local shear rate at the walls ($x = 0$ or 1) ranges from 0 at the center ($r = 0$) up to a normalized value of $3r/2$ at a normalized distance r from the center. According to Morris and Boulay [35] and considering only the effect of the shear rate gradient along a X-direction on particle migration, the characteristic shear deformation γ_c associated to particle migration is generated by the particle pressure gradient. Thus, it can be written $1/\gamma_c = (a^2/\eta_f V_0)(\partial \Pi/\partial X)$, where Π is the particle pressure and a the diameter of the particles. In our configuration, assuming the particle pressure scales as $\Pi \sim \eta_f \dot{\gamma} V_0/H$ and $X = xH$, it reduces to:

$$\frac{1}{\gamma_c} = \frac{a^2}{H^2}\frac{\partial \dot{\gamma}}{\partial x}. \quad (14)$$

Equation (13) allows to deduce that the shear rate gradient along the x-direction verifies the inequality $\partial\dot{\gamma}/\partial x < 3r$. This implies that the characteristic deformation for particles migration respects $\gamma_c > H^3/3\,a^2\,R$. Considering typical values of these parameters corresponding to the experiments presented above, $H = 10$ mm, $R = 80$ mm and $a = 0.5$ mm, the previous criteria becomes $\gamma_c > 17$. This characteristic deformation is larger than the typical deformation imposed in the squeeze experiment which is of order $R/H \simeq 5$. This confirms that particles migration is not significant in our experiments and the suspension can be assumed to be homogeneous.

Another known issue with squeeze flow geometry is the possible solid–liquid separation [27,28]. Phase separation occurs when the characteristic convection time of the suspension $\tau_c \propto 1/\dot{\gamma}$, which scales as H/V_0, is large compare to the characteristic time of the fluid flow through the particles (filtration) τ_w. As the filtra-

tion follows the Darcy's law, the filtration characteristic time scales $\tau_w \propto H^3/\eta_r(\phi)k(\phi)V_0$ where $k(\phi) = a^2(1-\phi)^3/(45\phi^2)$ is the Carman–Kozeny's permeability [36,37]. Thus the Peclet number defined as the ratio of τ_w and τ_c reads:

$$\mathrm{Pe} = \frac{45\,\phi^2\,(\phi_c-\phi)^2}{(1-\phi)^3\,{\phi_c}^2}\frac{H^2}{a^2} \tag{15}$$

If $\mathrm{Pe} \gg 1$, the filtration rate is low and the suspension remains homogeneous during the flow. On the contrary, if $\mathrm{Pe} \ll 1$, the filtration rate becomes significant and leads to particle/fluid separation. In the experiments presented above, an underestimate of the Peclet number is given by $\phi = 0.5$. It leads to minimal value of Peclet number $\mathrm{Pe} \simeq 1000$. Thus, the Peclet is always much larger than unity and no phase separation is expected in these conditions.

Furthermore, a major difference between Newtonian fluids and suspensions is the existence of normal stress differences in the suspension. These normal stress differences are a consequence of contact between solid particles, which induce additional stresses compared with the case of a pure fluid and lead to the dilatation of the suspension under shear. Several experimental [4,20,21,38] and theoretical [35] works present this normal stress effect. In our experimental configuration, the pressure sensor encodes the first normal stress difference N_1 (the difference between the normal stress in the flow and in the shear directions), whose signature should be a deviation from the usual effective viscosity of suspensions (Fig. 3) [35]. As we do not observe any deviation from Maron–Pierce law, we can conclude that $N_1 \simeq 0$. This is compatible with several experimental studies [4], also reporting that $N_1 \simeq 0$ for suspensions.

The last point concerns boundary conditions at the walls. In order to induce total slip conditions at the walls and generate a pure biaxial extensional flow, lubricated walls can be used [39]. This approach is limited by the fact that slip is often partial rather than perfect and is difficult to estimate experimentally. In the present study, we have considered no-slip conditions at the walls and the agreement between theory and experiments is correct. In future, it would be interesting to study how a change in boundary conditions affects the determination of the effective viscosity of a fluid in a squeeze flow.

4 Conclusion

In this study, we have considered a squeeze flow configuration as a viscometer. The squeeze flow is generated between a disk and a wall approaching at constant relative velocity. The fluid viscosity is deduced from the measurements of the radial pressure drop along the wall made with two pressure sensors. Indeed, the solution of the Navier–Stokes equations in a squeeze flow geometry and in the absence of inertia provides a linear relation between the radial pressure drop and the fluid viscosity. We have first validated this protocol with a Newtonian fluid whose viscosity has been estimated with a relative accuracy of 1 %. Then, this approach has been applied to a suspension of particles in order to determine its relative viscosity η_r regarding the suspending fluid. These experiments yield viscosity measurements in agreement with the Maron–Pierce law where the relative viscosity of the suspension evolves as $\eta_r \sim (1-\phi/\phi_c)^{-2}$. The critical packing fraction ϕ_c associated with the measurements in a squeeze flow is in good agreement with the one obtained from simple shear experiments. Thus, viscosity measurements made in a squeeze flow are consistent with the ones done in a simple shear flow cell, a result that reinforces the modeling of the suspension by a fluid of effective viscosity. Any characteristic phenomena of suspension flows such as shear-induced migration, liquid filtration or the presence of normal stress differences do not affect the viscosity measurement in a squeeze configuration. Finally, this work proves that the concept of effective viscosity for suspensions of particles is robust to a change in the flow geometry.

This work is based on local pressure measurements but it would be interesting in the future to investigate the fluid velocity field in order to test the validity of the theoretical prediction of this field when the fluid is a suspension of particles. Our approach to determine fluid viscosity has been proved to be efficient in the limit of small Reynolds number $\mathrm{Re} \ll 1$. It would be of interest to study the response of a suspension in a squeeze flow when the Reynolds number is not vanishingly small in order to address the role of inertia in this configuration.

Acknowledgements We are grateful to J. Amarni, A. Au bertin, L. Auffray, C. Manquest and R. Pidoux for their contribution to the development of the experimental setup. This work has been supported by "Investissements d'Avenir" LabEx PALM (Grant No. ANR-10-LABX-0039-PALM). We thank Anne Mongruel and Anniina Salonen for useful discussions.

Declarations

Declarations The authors have no relevant financial or nonfinancial interests to disclose. The authors contributed equally to the work. The datasets generated and analyzed during the current study are available from the corresponding author on reasonable request.

References

1. P. Coussot, *Mudflow rheology and dynamics* (Routledge, New York, 2017)
2. N. Roussel, *Understanding the rheology of concrete* (Elsevier, Amsterdam, 2011)
3. E. Blanco, D.J. Hodgson, M. Hermes, R. Besseling, G.L. Hunter, P.M. Chaikin, M.E. Cates, I. Van Damme, W.C. Poon, Proc. Natl. Acad. Sci. **116**(21), 10303 (2019)
4. É. Guazzelli, O. Pouliquen, J. Fluid Mech. **852** (2018)

5. A. Einstein et al., Ann. Phys. **17**(549–560), 208 (1905)
6. G. Batchelor, J. Fluid Mech. **52**(2), 245 (1972)
7. J.J. Stickel, R.L. Powell, Annu. Rev. Fluid Mech. **37**, 129 (2005)
8. P. Mills, P. Snabre, Eur. Phys. J. E **30**(3), 309 (2009)
9. P. Hébraud, Rheol. Acta **48**(8), 845 (2009)
10. A.C.K. Sato, R.L. Cunha, J. Food Eng. **91**(4), 566 (2009)
11. S. Olhero, J. Ferreira, Powder Technol. **139**(1), 69 (2004)
12. C. Gamonpilas, J.F. Morris, M.M. Denn, J. Rheol. **60**(2), 289 (2016)
13. S. Pednekar, J. Chun, J.F. Morris, J. Rheol. **62**(2), 513 (2018)
14. R. Mari, R. Seto, J.F. Morris, M.M. Denn, J. Rheol. **58**(6), 1693 (2014)
15. F. Peters, G. Ghigliotti, S. Gallier, F. Blanc, E. Lemaire, L. Lobry, J. Rheol. **60**(4), 715 (2016)
16. L. Lobry, E. Lemaire, F. Blanc, S. Gallier, F. Peters, J. Fluid Mech. **860**, 682 (2019)
17. R. Mari, R. Seto, J.F. Morris, M.M. Denn, J. Rheol. **58**(6), 1693 (2014)
18. A. Rashedi, M. Sarabian, M. Firouznia, D. Roberts, G. Ovarlez, S. Hormozi, AIChE J. **66**(12), e17100 (2020)
19. R. Seto, G.G. Giusteri, J. Fluid Mech. **857**, 200 (2018)
20. É. Couturier, F. Boyer, O. Pouliquen, É. Guazzelli, J. Fluid Mech. **686**, 26 (2011)
21. T. Dbouk, L. Lobry, E. Lemaire, J. Fluid Mech. **715**, 239 (2013)
22. S. Garland, G. Gauthier, J. Martin, J. Morris, J. Rheol. **57**(1), 71 (2013)
23. A. Singh, C. Ness, R. Seto, J.J. de Pablo, H.M. Jaeger, Phys. Rev. Lett. **124**(24), 248005 (2020)
24. J. Engmann, C. Servais, A.S. Burbidge, J. Nonnewton. Fluid Mech. **132**(1–3), 1 (2005)
25. J. Château, É. Guazzelli, H. Lhuissier, J. Fluid Mech. **852**, 178 (2018)
26. E.C. McIntyre, F.E. Filisko, Appl. Rheol. **19**(4), 44322 (2009)
27. N. Delhaye, A. Poitou, M. Chaouche, J. Nonnewton. Fluid Mech. **94**(1), 67 (2000)
28. J. Collomb, F. Chaari, M. Chaouche, J. Rheol. **48**(2), 405 (2004)
29. M. Nikkhoo, K. Khodabandehlou, L. Brozovsky, F. Gadala-Maria, Rheol. Acta **52**(2), 155 (2013)
30. W. Wolfe, Appl. Sci. Res. Sect. A **14**(1), 77 (1965)
31. D.C. Kuzma, Appl. Sci. Res. **18**(1), 15 (1968)
32. R. Grimm, Appl. Sci. Res. **32**(2), 149 (1976)
33. Q. Ghori, M. Ahmed, A. Siddiqui, Int. J. Nonlinear Sci. Numer. Simul. **8**(2), 179 (2007)
34. G.G. Giusteri, R. Seto, J. Rheol. **62**(3), 713 (2018)
35. J.F. Morris, F. Boulay, J. Rheol. **43**(5), 1213 (1999)
36. P.C. Carman, Discuss. Faraday Soc. **3**, 72 (1948)
37. E. Guyon, J.P. Hulin, L. Petit, C.D. Mitescu, *Physical hydrodynamics* (Oxford University Press, Oxford, 2015)
38. I.E. Zarraga, D.A. Hill, D.T. Leighton Jr., J. Rheol. **44**(2), 185 (2000)
39. S. Chatraei, C.W. Macosko, H. Winter, J. Rheol. **25**(4), 433 (1981)